Available online at www.sciencedirect.com

ScienceDirect

Procedia CIRP 41 (2016) 981 – 986

www.elsevier.com/locate/procedia

48th CIRP Conference on MANUFACTURING SYSTEMS - CIRP CMS 2015

Prediction of poly-methyl-methacrylate laser milling process characteristics based on neural networks and fuzzy data

Doriana M. D'Addona[a], Silvio Genna[b], Claudio Leone[a,b], Davide Matarazzo[a,*]

[a]*Department of Chemical, Materials and Production Engineering, University of Naples Federico II, P.le Tecchio 80, 80125 Naples, Italy*
[b]*CIRTIBS Research Centre, University of Naples Federico II, P.le Tecchio 80, 80125 Naples, Italy*

* Corresponding author. Tel.: +39-320-7173783. *E-mail address:* davide.matarazzo@unina.it

Abstract

Laser milling is a recent technology adopted in rapid prototyping to produce tool, mould and polymer-based microfluidic devices. In this process, a laser beam is used to machine a solid bulk, filling the area to be machined with a number of closely spaced parallel lines. Compared to traditional machining, this method has some advantages, such as: greater flexibility of use, no mechanical contact with the surface, a reduction in industrial effluents, a fine accuracy of machining, even with complex forms, and the possibility to work different kind of materials. While it is relatively easy to predict the depth of the area worked, the surface roughness is more difficult to predict due to the materials behaviors at microscopic level. This is truer when polymer processing is considered due to the local thermal effects. The paper addresses the application of an artificial neural network computing technique to predict the depth and the surface roughness in laser milling tests of poly-methyl-methacrylate. The tests were carried out adopting a CO_2 laser working in continuous and pulsed wave mode. The obtained results showed a good agreement between the model and the experimental data. As a matter of fact, despite the thermal degradation that occurs on the PMMA surface, neural network processing offers an effective method for the prevision of roughness parameters as a function of the adopted process parameters.

Peer-review under responsibility of the scientific committee of 48th CIRP Conference on MANUFACTURING SYSTEMS - CIRP CMS 2015

Keywords: Artificial intelligence; Laser milling; PMMA

1. Introduction

Laser milling is a recent technologies adopted in rapid prototyping to produce tool and mould [1-4]. Furthermore, it is also an effective technique to obtain polymer-based microfluidic devices [5-10]. In laser milling technique, a laser beam is used as a tool to machine a solid bulk, following predetermined patterns [4-19]. The material removal occurs layer by layer. Each layer is obtained by filling the area to be machined with a number of closely spaced parallel lines, sequentially machined in the materials. The thickness of the single layer is thin, so, in order to obtain a deep profile, the process has to be repeated up to the required depth. During the process, the geometry of the etched area can be changed in order to obtain complex profile (2D ½ sculpture). Compared to traditional machining processes, laser milling offers several advantages, including: greater flexibility of use, no mechanical contact with the surface, no tool wear, a reduction in industrial effluents (i.e. no acid, solvent or dielectric oils are required), a fine accuracy of machining, even with complex forms, and the possibility to work different kind of materials such as metals [11-14], wood [17], composite [18], ceramics [4,19] and polymers [7-12].

However, the Material Removal Rate (MRR), the heat affected zone, the surface roughness, as well as, the interaction phenomena occurring during the milling process, strictly depend on the material properties, the laser source characteristics, comprises the wavelength, and the process parameters [4-19]. In a previous works, the authors have shown that the depth and the machined volume linearly depend on the total amount of released energy [11-14, 17, 18]. On the contrary, the surface roughness depends in a complex way on average power, adopted step, the wave mode and the scanning speed [7-18]. Consequently the roughness estimation involves the knowledge of the different mechanisms of surface formation and their dependence on the process parameters. Since the material removal is based on the realization of single grooves placed one alongside one another, the development of

Peer-review under responsibility of the scientific committee of 48th CIRP Conference on MANUFACTURING SYSTEMS - CIRP CMS 2015
doi:10.1016/j.procir.2016.01.029

a model, able to estimate the depth and the roughness, starts from the estimation of the shape of the groove as a function of the process parameters. In [5] an experimental model for the channel depth prediction as a function on the process parameters was presented. The model assumes that the ablated material depth is proportional to the amount of heat (Q) that is available to vaporize the polymer material. This heat is given as the absorbed energy (Q_{in}) coming from the laser that is higher than a certain threshold (Q_{th}), i.e.:

$$Depth = kQ = k(Q_{in} - Q_{th}) \quad (1)$$

where k is a proportionality constant that is related to the vaporisation energy of the material. While the term (Q_{th}) represents the threshold heat i.e. the energy losses in the process needed to heat up the irradiated spot and its surroundings before ablation begins, as well as the energy that is lost due to heat conduction into the surroundings.

This type of relationship is very effective, because allows to directly related the depth to the released energy. Furthermore, it can be directly applied the prevision of the pocket depth obtained in laser milling for different materials, such as metals alloy [11-14], wood [17], composite [18], ceramics [4,19] and Poly-Methyl-MethAcrylate PMMA [11,12].

In [7] L. Romoli et al. present an empirical formulation in order to predict the groove width as a function of Average Power/Scan Speed ratio (P_a/S_s), the beam spot diameter, a threshold energy below which no vaporization occurs by the equation and an experimental constant. The models have been applied in [8] to predict the depth and Rt roughness parameters of the machined area. It was assumed that the groove generated on the material had a triangular shape. This assumption goes well when using high ratio P_a/S_s, like in [7-8], while does not fit to reality when the ratio P_a/S_s is low and the shape of the groove is more similar to a half circle, like as in the present study, Fig 1. In the real process, the groove shape depends on the energy distribution of the laser, and, for a laser source with a Gaussian energy distribution, is very close to the shape of the energy distribution (i.e. a Gaussian shape).

In [9] Jensen et al. suggest to model the groove shape by fitting the Gaussian function to the profile of a channel created by a single pass of the laser beam. Then the overall profile obtained in the milling process could be calculated by the superposition of the groove produced in each beam travel. However the model was not applied to predict the roughness. A similarly approach was adopted in [12]. In this case the geometry of the single groove was estimate adopting a semi-empirical model able to estimate the groove shape. Then, the profile of the etched area were predicted by superposition of the grooves geometry estimate by the semi-empirical model based on energy considerations. From the results a good agreement between the estimates etched area depth and the experimental data were found.

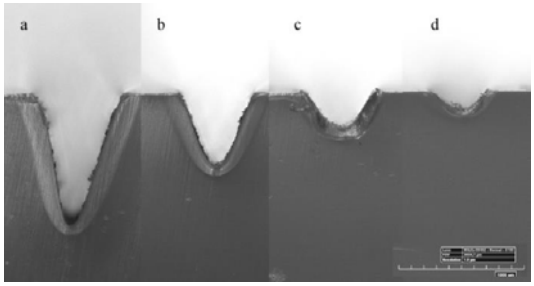

Fig. 1. Section of groves obtained at CW mode, P_a=30W and a scan speed (mm/s) of: (a) 25; (b) 50; (c) 100; (d) 200.

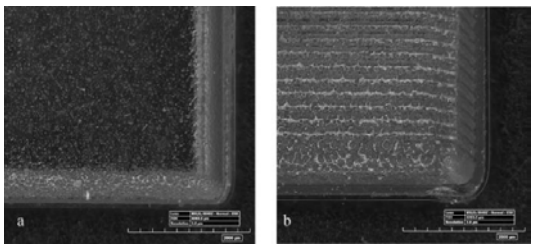

Fig. 2. Images of samples obtained at CW mode, P_a=30W and (a) S_s=600 (mm/s) step=0.05 mm; (b) S_s=50 (mm/s) step=0.2 mm.

However, the proposed model was not able to estimate the roughness because does not take in account the thermal damage that occurs into the material. As a matter of fact, the resulting roughness depended only partly on the pure ablative terms, and the model does not take in account the consequence of phase transformation and polymer degradation phenomena. The increase of the temperature, due to the energy lost by heat conduction produces different phenomena in the surrounding of the machined area, such as: melting, softening and relaxation and bubbling/boiling [20-23]. The viscous material is pushed and ejected by the gas vapour phase produced during the ablation. This material is resolidified at the side of the groove producing bulges at the rim of the groove [12, 20-22]. The material, due to the temperature increase, produces relaxation in the molecular chain, with consequent change in the machined profile. During the machining, the decomposition of PMMA occurs also in the molten and in the softened phase, consequently vapour phase may be formed and may expand from the internal regions of the polymer. The volatile decomposed products nucleate within the liquid and PMMA layer forming bubbles that increase in size and finally explode on the surface producing porosity [12, 21-23] as visible in Fig 2, where images of etched surfaces obtained in different conditions are reported. All these phenomena involve a change in the geometry of the pocket at the micro level which is reflected on the final roughness.

On the other hand, the ability of the Artificial Neural Network (ANNs) in the prediction of complex systems is well known. ANNs are able to learn from examples, understand the environment in which they operate by finding functional relationships among different given inputs and, eventually, produce an output. D'Addona et al. [24] investigated the ANN performances in the forecasting of cutting tool wear of Ni-base

alloy components. The accurate correct prediction of such outputs, might allow the right selection of working parameters. Leone et al. [25] conducted studies to predict the residual stress strength of glass fibre-reinforced plastic beams pre-fatigued via the training of ANNs and taking as input the acoustic emission (AE) signal recorded during the process. In order to define the best process parameters, Xu et al. [19] predicted the laser milling quality of $A1_2O_3$ ceramics with ceramics features, by relating process input features with the milling parameters depth and width.

The present paper addresses the application of an Artificial Neural Network (ANN) computing technique to predict the depth and the surface roughness in laser milling tests of poly-methyl-methacrylate. The tests were carried out adopting a CO_2 laser working in continuous and pulsed wave mode, CW and PW respectively. Several ANN configurations were trained to optimize the forecast of the milling parameters. In this study are presented two different ANN training functions, which were trained with different methods and network configurations.

The obtained results showed a good agreement between the model and the experimental data. As a matter of fact, despite the thermal degradation that occurs on the PMMA surface, neural network processing offers an effective method for the prevision of roughness parameters as a function of the adopted process parameters.

2. Equipment, material and experimental procedures

2.1. Equipment

The tests were performed using a sealed 30W RF excited CO2 laser source (Fly 30 CO2 by LASIT) working at the fundamental wavelength of 10˙600 nm. The laser beam is moved through two galvanometric mirrors, then it is focused by a "flat field" lens with a focal length of 100 mm onto the sample surface. The laser system is computer controlled, which allows the generation of the geometric patterns and the set up of the process parameters: average power (Pa); scan speed (Ss); wave mode: continuous wave and the pulsed wave and, in the pulsed regime, the pulse frequency (F). In pulsed wave mode, for a fixed average power, the pulse energy (i.e., the energy released in a single pulse, also namely Pe) depends on pulse frequency by way of the well known relation: Pe=Pa/F. Pulse energy, together to the pulse power, plays a central role in laser machining and micromachining since they determine the laser beam-material interaction mode, the amount of machined volume, the roughness and thermal damage extension [11-19, 26-29].

Accordingly, it was chose to use two different conditions for the PW regime, corresponding to the two frequencies: 2 and 15 kHz. At these frequencies, the two pulse energy values, far from each other, of 13.8 and 1.9 mJ were obtained. On the other hand, it is worth noting that frequency and scanning speed affect the so-called overlapping factor that is another critical parameter for pulse laser applications. Table 1 shows the detailed characteristics of the laser system.

2.2. Materials

The adopted material was a commercial (PMMA) plate, 3 mm in thickness. This material is especially advantageous for this application thanks to the perfect mix of features, such as: high absorptions of the radiation at the CO_2 wavelength (about 92% at 10˙600 nm [5, 30]), low heat capacity and low heat conductance, low transition temperature (in the range of 95-120°C [31]), and low degradation temperature (350 – 380 °C). When irradiated by the laser beam, the PMMA absorbs about all the radiation and rapidly increases its temperature up to the degradation one. At this temperature, vaporization occurs by random breaking and end-chain scission, producing a volatile phase made of PMMA monomers and CO_2 vapours [10, 32, 33]. The process without any chemical degradation or carbonisation occurs, so it is called non-charring pyrolysis [34]. Consequently, the process is very efficient (it mean that the loss in energy is very low), and the machined surfaces could be smooth, clean and HAZ free [6, 20, 21].

2.3. Experimental procedures

The experimental tests were carried out etching pockets of 10x10 mm^2 on PMMA samples of 60x60x3 mm^3 in size. On each sample, 9 areas were etched at the maximum average power (P_a), by filling the area with parallel lines, changing the parameters: wave mode (CW or PW), scan speed (S_s), space between the parallel lines (step or st). The adopted process parameters were selected on the basis of preliminary tests, taking in account also the released energy. In particular, to avoid the beam defocusing, and then an excessive decrease of the energy density, the energy released during the overall test was limited at 300 J. This results in the selection of an appropriate combination of Step and scanning speed. In Table 3 the adopted process conditions for the milling tests are reported, while in Fig. 1 the typical appearance of a sample and tasks are reported. No less of 4 samples were carried out for each process condition. To measure the depth of the pocket and the roughness, a 3D Surface Profiling System (Talysurf CLI 2000 from Taylor Hobson).

Table 1. Laser source characteristics.

Characteristics	Value	Units
Source type	RF excited CO_2 (Fly 30 CO_2)	--
Wavelength	10˙600	[nm]
Nominal average power	30	[W]
Pulse frequency	CW or 1-10	[kHz]
M2 factor	≈ 1.2	--
Focal length	100	[mm]
Declared focal spot	$\phi \approx 220$*	[μm]

Table 2. Process condition adopted in the milling test.

Regime	Step [mm]	Scanning speed [mm/s]	Released energy [J]
CW	0.05	600	100
		1200	50
	0.1	300	100
		600	50
PW 2 kHz	0.2	50	300
		75	200
PW 15 kHz		150	100
		300	50
		600	25

The system was equipped with an inductive gauge 2 µm radius diamond stylus, was adopted. Profiles of 14 mm in length were acquired orthogonally to the beam direction over the whole pocket profile. An axis resolution of 0.5 µm, a lateral resolution of 0.5 µm and a vertical resolution of 8.28 nm were adopted. No less than 4 profiles were recorded for each pocket. In order to discriminate the different surface characteristics, the arithmetic mean of the deviations from the mean (R_a) and the total height of the roughness profile (R_t) were adopted.

2.4. Neural network configuration set-up

In order to predict the best output, from a given input, it was chosen to work with Back Propagation Neural Networks (BP NN) [35], because they are able to understand functional relationships between given inputs and outputs [36].

The *casadeforwardnet* (CFN) function is a BP NN, which has the following MATLAB R2014b syntax:

cascadeforwardnet(hiddenSizes,trainFcn) (2)

The particularity of the cascadeforwardnet function is a weight connection from the input and every previous layer to the following layers and the three-layer network also has connections from the input to all three layers. The CFN was trained with the Training-Validation-Testing (T-V-T), by setting the Training as the 70% of the input data, Validation as the 15% and Test as the remaining 15%, while the best number of hidden nodes was chosen by trial, as indicated in Table 3. MATLAB randomly divides these three sets.

To achieve the best ANN performances [36], they have been also trained by using the *newcf* (N_CF) function, which is a BP NN, and it was also run in MATLAB R2014b, according to the following code:

net = newcf (P', T', [S1 S_i], {TF1 TF2…TF_N}) (3)

Where:

- newcf: function to create a cascade-forward BP network;
- P': to transpose input matrix or array: R x Q1 matrix of Q1 sample R-element input vectors;
- T': to transpose target matrix or array: S_N x Q2 matrix of Q2 sample SN-element input vectors;
- S_i: number of input and output layers: size of i^{th} layer, for N-1 layers;
- TFN: to transfer function of the i^{th} layer.

The formula in (3) returns a three-layer cascade-forward BP network: as setting, it was chosen as transfer function, between input and hidden layer, the tangent sigmoid, while, to produce the output a linear function was chosen. The best number of nodes were chosen by trial, as shown in Table 3. The size of the output layer varied among 1, 2 and 3: it depended by the type of chosen output: one to predict the single value of R_a, R_t and depth, two for the simultaneous prediction of R_a and R_t, 3 to predict simultaneously R_a, R_t, depth. The ANN input parameters consist of time, scan speed, wave mode, steep, average power and total released energy.

The input data matrix was pre-processed by randomly applying a noise (±2.5%) to the input values of scan speed, wave mode, steep, average power and total released energy. This procedure was required to avoid overfitting problems, which might be caused by the large size of the input matrix.

In order to test the performances of the newcf ANNs, the leave-k-out (L-k-O) method was been applied by setting *k = 1*, and this means that the Training phase was carried out with the full input matrix, with the exception of the testing row *k*.

In Table 3 the configuration of the tested ANN are summarised. The ability to estimate the depth and the roughness of the ANNs, was estimate by mean of the parameter "successful rate percentage" (Sr%) calculated as:

$$Sr\% = \left[1 - \left(\frac{1}{n}\sum_{i=1}^{n}\frac{|F_k - A_k|}{A_k}\right)\right] \times 100 \quad (4)$$

Sr% was calculated as the percentage of the ones' complement of the Mean Absolute Percentage Error (MAPE) [37], where A_k is the actual value, F_k the predicted one and *n* the dimension of training set. The MAPE indicates the accuracy as a percentage of data.

Table 3. Tested ANN configuration.

ANN ID	NET	Nodes	Method	% training	k	Tr. set
1	CFN	5	T-V-T	70-15-15	#	114
2	CFN	33	T-V-T	70-15-15	#	114
3	CFN	25	T-V-T	70-15-15	#	114
4	CFN	40	T-V-T	70-15-15	#	114
5	CFN	45	T-V-T	70-15-15	#	114
6	CFN	10	T-V-T	70-15-15	#	114
7	N_CF	7	L-k-O	FULL - k	1	114
8	N_CF	3	L-k-O	FULL - k	1	114
9	N_CF	48	L-k-O	FULL - k	1	114
10	N_CF	15	L-k-O	FULL - k	1	114
11	N_CF	5	L-k-O	FULL - k	1	114
12	N_CF	27	L-k-O	FULL - k	1	114
13	N_CF	10	L-k-O	FULL - k	1	114
14	N_CF	25	L-k-O	FULL - k	1	114
15	N_CF	20	L-k-O	FULL - k	1	114
16	N_CF	30	L-k-O	FULL - k	1	114

3. Results and discussion

In Figures 3-5, the success rate for R_a, R_t and depth vs. the ANN ID are reported. From the Figures it is clearly visible that the success rate depend on the ANN architecture, the number of the adopted nodes, the number of output and the investigate parameters. Generally speaking the CFNs (ID=1-7) show a better response in the depth and R_a prediction compared to the N_CFs (ID=7-12). By examining the ANN performance for each single parameters (R_a, R_t and Depth) it can be deduced that the network n°5 shows the better response for all the three parameters and for both output configuration (single or triple).

In Figures 6-8, the R_a, R_t and depth predicted by the 1-output ANN_ID n°5, were reported against the measured ones, respectively. While in Figs. 9-11, the same diagrams are reported for the 3-output ANN_ID n°5. From the figures, despite the use of fuzzy data, almost all the points are fairly closed to the 45° straight line (i.e. the dashed line). This means that a good agreement between the experimental and estimated values was obtained. Adopting a 1-output ANN a MAPE a greater than 87% was obtained for all the parameters. Moreover, compared to a 3-output ANN, the use of a 1-output ANN, results in an improvement of the MAPE of about 10%.

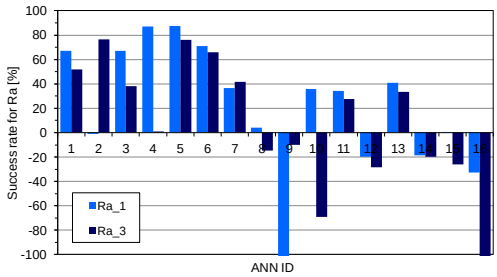

Fig. 3. Success rate for R_a obtained for the different NN_ID.

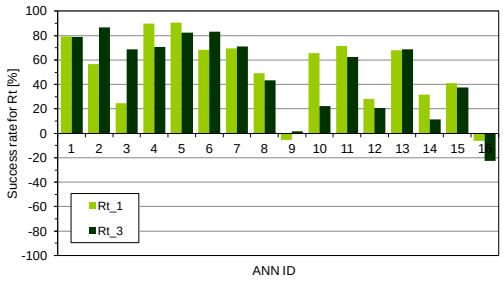

Fig. 4. Success rate for R_t obtained for the different NN_ID.

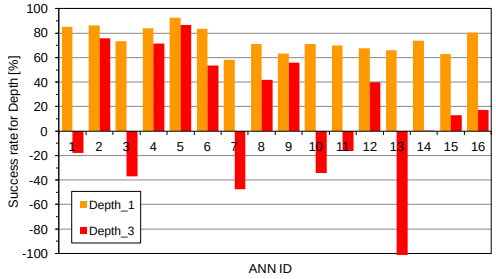

Fig. 5. Success rate for the depth obtained for the different NN_ID.

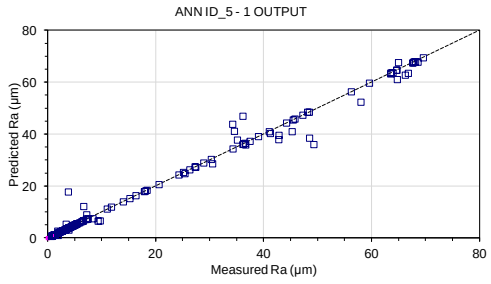

Fig. 6. Predicted R_a against measured R_a, CFN, 45 nodes, 1 output.

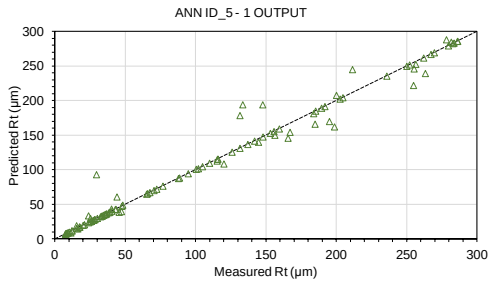

Fig. 7. Predicted R_t against measured R_t, CFN, 45 nodes, 1 output.

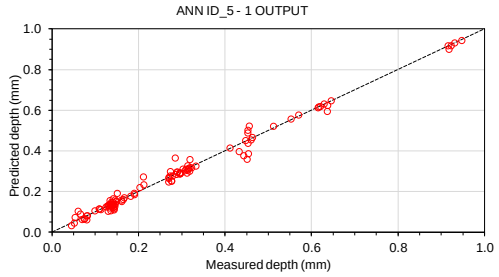

Fig. 8. Predicted depth against measured depth, CFN, 45 nodes, 1 output.

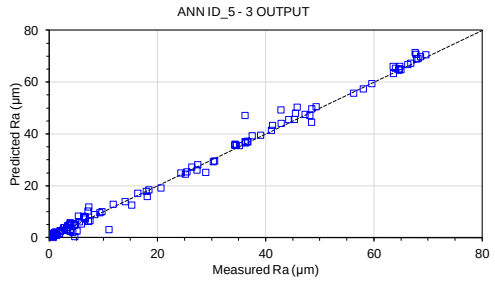

Fig. 9. Predicted R_a against measured R_a, CFN, 45 nodes, 3 outputs.

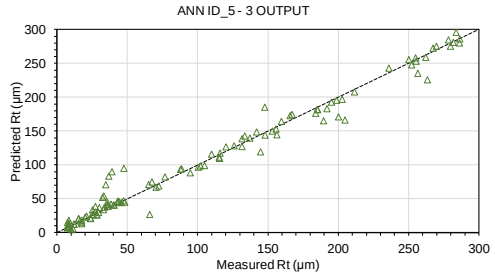

Fig. 10. Predicted R_t against measured R_t, CFN, 45 nodes, 3 outputs.

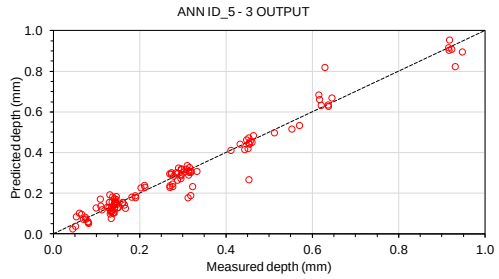

Fig. 11. Predicted depth against measured depth, CFN, 45 nodes, 3 outputs.

4. Conclusion

Artificial Neural Network computing technique was applied to estimate the depth and the surface roughness on of PMMA samples obtained by laser milling tests. From the obtained results, the main conclusions are as follows.

Despite the use of fuzzy data, it was proven that the ANNs are able to describe the relation between the process parameters

and the depth and the roughness obtained in the laser milling operation of PMMA.

The depth and the surface roughness (Ra, Rt) were best estimated by training a Cascadeforwadnet with 45 nodes in hidden layer and by utilizing the T-V-T method for training.

The analysis shows good results in terms of MAPE, which means that the model has good precision compared to the former studies reported in bibliography.

Compared to a 3-output ANN, the use of a 1-output ANN, results in an improvement of the MAPE of about 10%.

Acknowledgements

The authors are grateful to the CIRTIBS Research Centre of the University of Naples Federico II, for providing the equipment and the financial support to the research.

References

[1] Kaldos A, Pieper HJ, Wolf E, Krause M, Laser machining in die making - A modern rapid tooling process, J. of Materials Processing Technology, 2004; 155–156: 1815-1820.
[2] Ready JF, LIA Handbook of Laser Materials Processing Springer-Verlag Berlin and Heidelberg GmbH & Co. K, 2001.
[3] Klank H, Kutter JP, Geschke O, CO_2-laser micromachining and back-end processing for rapid production of PMMA-based microfluidic systems, Lab on a Chip - Miniaturisation for Chemistry and Biology, 2002; 2/4: 242-246.
[4] Leone C, Quadrini F, Santo L, Tagliaferri V, Trovalusci F, Nd-YAG laser sculpture of WC punches for micro-sheet forming, Key Engineering Materials, 2007; 344: 783-789.
[5] Huang Y, Liu S, Yang W, Yu C, Surface roughness analysis and improvement of PMMA-based microfluidic chip chambers by CO_2 laser cutting, Applied Surface Science, 2010; 256: 1675-1678.
[6] Snakenborg D, Klank H, Kutter JP, Microstructure fabrication with a CO2 laser system, J. of Micromechanics and Microengineering, 2004; 14: 182-189.
[7] Romoli L, Tantussi G, Dini G, Layered Laser Vaporization of PMMA Manufacturing 3D Mould Cavities, Annals of the CIRP, 2007; 56: 209-212.
[8] Romoli L, Tantussi G, Dini G, Experimental approach to the laser machining of PMMA substrates for the fabrication of microfluidic devices, Optics and Lasers in Engineering, 2011; 49: 419–427.
[9] Jensen MF, Noerholm M, Christensen LH, Geschke O, Microstructure fabrication with a CO2 laser system: characterization and fabrication of cavities produced by raster scanning of the laser beam, Lab on a Chip - Miniaturisation for Chemistry and Biology, 2003; 3/4: 302-307.
[10] Holland BJ, Hay JN, Surface roughness analysis and improvement of PMMA-based microfluidic chip chambers by CO2 laser cutting, Polymer Degradation and Stability, 2002; 77: 435-439.
[11] Genna S, Leone C, Lopresto V, Tagliaferri V, Experimental investigation on laser milling of PMMA sheet, AIP Conference Proceedings, 2014; 1599: 242-245.
[12] Genna S, Leone C, Lopresto V, Tagliaferri V, An experimental study on the surface mechanisms formation during the laser milling of PMMA, Polymer Composites, Article first published online: 28 MAR 2015, DOI: 10.1002/pc.23442.
[13] Genna S, Leone C, Lopresto V, Santo L, Trovalusci F, Study of fibre laser machining of C45 steel: Influence of process parameters on material removal rate and roughness, Int. J. of Material Forming, 2010; 3/1: 1115-1118.
[14] Leone C, Morace RE, De Iorio I., AISI 304 stainless steel engraving by Q-switched Nd:YAG nanosecond laser, J. of the Chinese Society of Mechanical Engineers, 2007; 28/2: 217-224.
[15] Campanelli SL, Ludovico AD, Bonserio C, Cavalluzzi P, Cinquepalmi M, Experimental analysis of the laser milling process parameters, J. of Materials Processing Technology, 2007; 191: 220-223.
[16] Campanelli SL, Contuzzi N, Casalino G, Ludovico AD, Analysis of the material removal rate of nanosecond laser ablation of aluminium using a parallel hatching mode, Applied Mechanics and Materials, 2012; 201-202: 1159-1163.
[17] Leone C, Lopresto V, De Iorio I, Wood engraving by Q-switched diode-pumped frequency-doubled Nd:YAG green laser, Optics and Lasers in Engineering, 2009; 47/1: 161-168.
[18] Leone C, Papa I, Tagliaferri F, Lopresto V, Investigation of CFRP laser milling using a 30 W Q-switched Yb:YAG fiber laser: Effect of process parameters on removal mechanisms and HAZ formation, Composites: Part A, 2013; 55: 129-142.
[19] Xu ZM, Hong ZH, Experimental Investigation on Laser Milling of Al_2O_3 Ceramic, Applied Mechanics and Materials, 2014; 457-458: 160-163.PMMA New
[20] Malek CGK, Laser processing for bio-microfluidics applications (part I), Analytical and Bioanalytical Chemistry, 2006; 385: 1351-61.
[21] Malek CGK, Laser processing for bio-microfluidics applications (part II), Analytical and Bioanalytical Chemistry, 2006; 385: 1362–69.
[22] Efthimiopoulos T, Kiagias C, Heliotis G, Helidonis E, Evidence of volume bubble creation during laser ablation of PMMA organic polymer, Canadian Journal of Physics, 2000; 78/5-6: 509-519.
[23] Sakatsuji W, Konishi T, Miyamoto Y, Effects of thermal history on enthalpy relaxation: Annealing effect in polymethylmethacrylate, Journal of Thermal Analysis and Calorimetry, 2013; 113/3: 1129-1134.
[24] Leone C, D'Addona DM, Teti R, Tool Wear Modelling through Regression Analysis and Intelligent Methods for Nickel Base Alloy Machining, CIRP Journal of Manufacturing Science and Technology, 2011; V4/3: 327-331.
[25] Leone C, Caprino G, De Iorio I, Interpreting acoustic emission signals by artificial neural networks to predict the residual strength of pre-fatigued GFRP laminates, Composites Science and Technology, 2006; 66/2: 233-239.
[26] Leone C, Genna S, Caprino G, De Iorio I, AISI 304 stainless steel marking by a Q-switched diode pumped Nd:YAG laser, Journal of Materials Processing Technology, 2010; 210/10: 1297-1303.
[27] Leone C, Genna S, Tagliaferri V, Fibre laser cutting of CFRP thin sheets by multi-passes scan technique, Optics and Lasers in Engineering, 2015; 53: 43-50.
[28] Lutey AHA, Fortunato A, Ascari A, Carmignato S, Leone C, Laser cutting of lithium iron phosphate battery electrodes: Characterization of process efficiency and quality, Optics and Laser Technology, 2015; 65: 164-174.
[29] Leone C, Genna S, Caggiano A, Resource efficient low power laser cleaning of compact discs for material reuse by polycarbonate recovery, CIRP Journal of Manufacturing Science and Technology, 2015; 9: 39-50.
[30] Atanasov P.A., Baeva M.G., CW CO2 laser cutting of plastics, Proceedings of SPIE, 1997; 3092, 772-775.
[31] Nayak NC, Lam YC, Yue C.Y., Sinha AT, CO2-laser micromachining of PMMA: the effect of polymer molecular weight, Journal of Micromechanics and Microengineering, 2008; 18/9: art. n° 095020.
[32] Arisawa H, Brill TB, Kinetics and mechanisms of flash pyrolysis of poly (methyl methacrylate) (PMMA), Combustion and Flame, 1997; 109: 415-26.
[33] Ferriol M, Gentilhomme A, Cochez M., Oget N., Mieloszynski J.L., Thermal degradation of poly (methyl methacrylate) (PMMA): modelling of DTG and TG curves, Polymers Degradation Stability 2003; 79: 271-81.
[34] Jia F, Galea ER, Patel MK, The numerical simulation of the noncharring pyrolysis process and fire development within a compartment, Applied Mathematical Modelling, 1999; 23: 587-607.
[35] D'Addona DM, Matarazzo D, Sharif Ullah AMM, Teti R, Tool Wear Control through Cognitive Paradigms, Procedia CIRP, Volume 33, 2015, Pages 221-226, ISSN 2212-8271, http://dx.doi.org/10.1016/j.procir.2015.06.040.
[36] D'Addona DM, Matarazzo D, Di Foggia M, Caramiello C, Iannuzzi S, Inclusion Scraps Control in Aerospace Blades Production through Cognitive Paradigms, Procedia CIRP, Volume 33, 2015, Pages 322-327, ISSN 2212-8271, http://dx.doi.org/10.1016/j.procir.2015.06.070.
[37] Chin Wang Lou, Ming Chui Dong, A novel random fuzzy neural networks for tackling uncertainties of electric load forecasting, International Journal of Electrical Power & Energy Systems, 2015; 73: 34-44.